

Prestack migration by equivalent offsets and CSP gathers

John C. Bancroft, Hugh D. Geiger, Gary F. Margrave, Shaowu Wang, and Darren S. Foltinek

ABSTRACT

A method of prestack time migration is presented that is simpler, faster, and provides better velocity information than conventional methods. It is based on prestack Kirchhoff time migration and can be applied to both 2-D and 3-D data. The method is divided into two steps, a gathering process that forms common scatterpoint (CSP) gathers, and an imaging process using a Kirchhoff migration performed independently on each CSP gather.

The CSP gathering process sums input traces into equivalent offset bins in each CSP gather with *no* time shifting. The *equivalent offset* is defined by an exact algebraic transformation of the double square root (DSR) equation of prestack time migration into a hyperbolic form. A CSP gather is similar to a CMP gather as both contain offset traces, and both represent a vertical array of scatterpoints. CSP gathers can be formed at any arbitrary location, have higher fold in their offset bins, and have a much larger offset range due to the gathering of all input traces within the migration aperture.

The imaging process collapses each CSP gather into a single migrated output trace. It is performed as a Kirchhoff process which consists of scaling, filtering, normal moveout (NMO) correction, and stacking. The migration velocities are determined by conventional velocity analysis of the CSP gathers.

Significant computational savings result from delaying arithmetic operations on the input samples until after the CSP gather has been formed. The high fold and large offsets of the CSP gather provide better focusing and improved velocity analysis. This space-time domain method is suitable for uneven geometries, enables velocity analysis at random locations, and permits prestack migration of a 3-D volume into an arbitrary 2-D line. It may also be adapted to migrate from topography, and to migrate converted wave (P-SV) data.

Results from conventional processing of real 2-D and 3-D data are compared with the new method, demonstrating improved velocity analysis and superior migrated images.

INTRODUCTION

Migration is a process that attempts to reconstruct an image of the earth's reflecting structure from elastic wavefield energy recorded at the surface in seismic traces. Since the invention of the CMP processing method (Mayne, 1962), *conventional processing* has concentrated on producing a stacked section from common midpoint (CMP) gathers, followed by a poststack migration based on the stacking velocities. Stacking velocities generally differ from those required for poststack migration, and

some form of migration velocity estimation is usually required. Further processing advances recognized that dip dependent stacking velocities and reflection point smearing could be corrected by the inclusion of dip moveout (DMO) (Hale 1984, Deregowski 1986) or prestack migration (Shultz and Sherwood 1980, Sattlegger et al. 1980). The use of these prestack processes in velocity analysis loops enabled a more accurate estimate of the subsurface velocities and improved subsurface images.

DMO and poststack migration are currently more economical than typical methods of prestack migration; consequently, in areas with smooth velocities, DMO tends to be the current processing standard. In areas where the smooth velocity criteria fails, prestack migration should be the preferred processing method. Typical prestack migration methods include migration of source records (Schultz and Sherwood 1980, Reshef and Kosloff 1986, van der Schoot et al. 1989, Lee and Zhang 1992, Ng 1994), migration of constant (or limited) offset sections (Sattlegger et al. 1980, Deregowski 1990), and migration by alternating downward continuation between shot gathers and geophone gathers (Denelle et al. 1986, Diet et al. 1993). This paper will refer to *full* prestack Kirchhoff migration (Lumley 1989, Lumley and Claerbout 1993) as the scaled and filtered summation of input samples along a defined trajectory for each output migrated sample. The historical basis of prestack migration dates back to the early 1970's, as described in papers by Lindsey and Herman (1970) and Rockwell (1971). The common use of full prestack migration continues to be limited by computer hardware and long run times.

The method presented in this paper is based on the principles of full prestack Kirchhoff time migration. An intermediate step in the process forms prestack migration gathers at each migration output location with traces sorted by a new offset measure called *equivalent offset*. The gathers are formed with no time shifting, and scattered energy is aligned with hyperbolic moveout. After the gathers have been formed, a Kirchhoff migration of each CSP gather to a zero offset trace completes the prestack migration. This new method is called *equivalent offset* migration (EOM) with initial results reported by Bancroft and Geiger (1994), Bancroft et al. (1994), Bancroft and Wang (1994), Geiger et al. (1995), and Bancroft et al. (1995).

A companion paper (Margrave et al. 1996) provides mathematical rigor by deriving a parallel method called *equivalent wavenumber* migration (EWM) from the Fourier transform theory established by Stolt (1978). EWM is shown to be an *exact* reformulation of prestack FK migration, and EOM is its Kirchhoff time domain implementation.

Prestack migration model

The full Kirchhoff approach to prestack migration is based on a model of scatterpoints which scatter energy from any source to all receivers (in contrast to specular reflections assumed by the CMP method). Huygens principle implies that an organized arrangement of scatterpoints will produce a coherent reflection event. The surface position of a vertical array of scatterpoints is referred to as the *common scatterpoint* (CSP) location. The objective of prestack migration is to gather all of the

scattered energy and relocate it to the position of the scatterpoints. The traditional concept of full prestack Kirchhoff migration assumes an output scatterpoint, and then gathers the appropriate energy from all available input traces. This procedure is repeated for every output scatter point.

The time of scattered energy in each input trace (relative to a scatterpoint) is identified by the traveltime along the raypaths between the source, scatterpoint, and receiver. Raypath traveltimes may be estimated by a number of different methods, such as hyperbolic computations for *time* migration or wavefront computations for *depth* migration. After time migration the samples in a trace follow the trajectory of an image ray (Hubral and Krey 1980, Black and Brzostowski 1991). This concept of an image ray allows a time migration to be converted to an estimate of a depth migration.

Scatterpoint traveltimes - Cheop's pyramid

Most full prestack Kirchhoff time migrations assume linear ray paths from the source to scatterpoint, and from the scatterpoint to receiver as illustrated in Figure 1. The total traveltime T is estimated from the source to scatterpoint time T_s , and the scatterpoint to receiver time T_r by

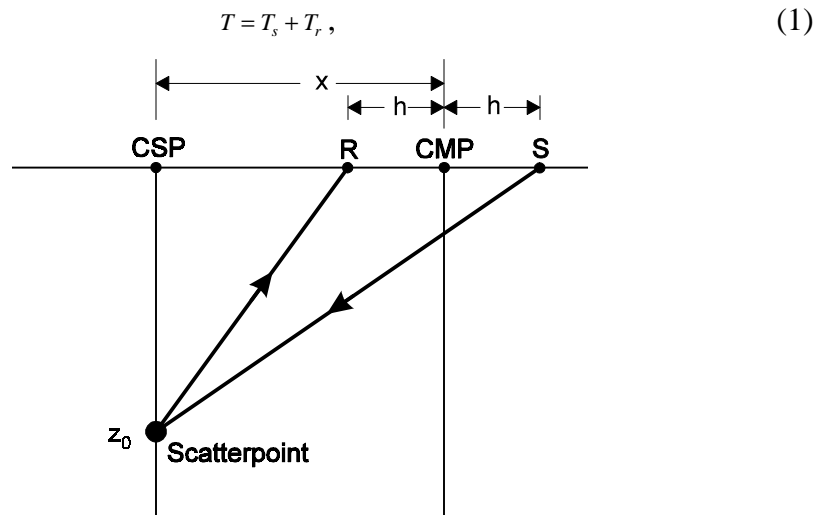


FIG. 1. Geometry for prestack Kirchhoff time migration showing a raypath from source S to receiver R via a scatterpoint.

From the geometry of Figure 1, and assuming (for the moment) that the velocity V is constant, these terms define the double square root (DSR) equation

$$T = \left[\frac{z_0^2 + (x+h)^2}{V^2} \right]^{1/2} + \left[\frac{z_0^2 + (x-h)^2}{V^2} \right]^{1/2}, \tag{2}$$

where z_0 is the depth of the scatterpoint, x the distance from the common midpoint (CMP) to the common scatterpoint (CSP), and h is the half source-receiver offset. Extending equation (2) to include a variable migration velocity V_{mig} gives

$$T = \left[\left(\frac{T_0}{2} \right)^2 + \frac{(x+h)^2}{V_{mig}^2} \right]^{1/2} + \left[\left(\frac{T_0}{2} \right)^2 + \frac{(x-h)^2}{V_{mig}^2} \right]^{1/2}, \quad (3)$$

where the migration velocity is the RMS approximation of Tanner and Koehler (1978) evaluated at time $T_0 = T(x=0, h=0)$. T_0 is the two-way zero offset time computed from the average velocity V_{ave} as

$$T_0 = \frac{2z_0}{V_{ave}}. \quad (4)$$

The DSR equation may be used to compute the traveltime T for one scatterpoint at T_0 into a continuum of 2-D x and h locations as shown in Figure 2a. This surface is known as Cheop's pyramid (Claerbout 1984 pages 164-163). Cheop's pyramid is the prestack migration equivalent to the zero offset hyperbola of 2-D poststack migration. For comparison purposes, a hyperboloid for the same scatterpoint is shown in Figure 2b. The left side of Figure 2a illustrates the non-hyperbolic moveout in a CMP gather offset from the scatterpoint and can be compared with the hyperbolic shape on the left side of the hyperboloid of Figure 2b.

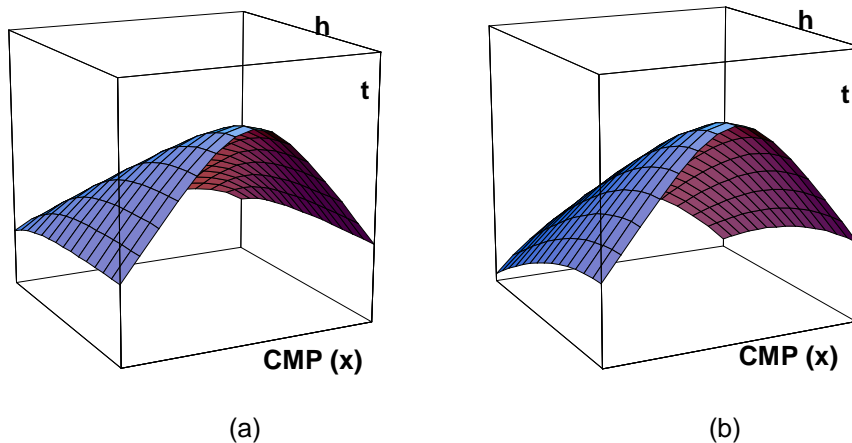


FIG. 2. Perspective view of (a) Cheop's pyramid defined by the DSR equation (6) and (b) an hyperboloid created from the same scatterpoint.

The migration velocity for Cheop's pyramid is defined at the apex, regardless of the spatial or temporal extent of the scattered energy. The Cheop's pyramid is a useful visualization for 2-D scattered energy but is not applicable to 3-D data. A technique for handling the 3-D case will be presented later in this paper.

Kirchhoff prestack imaging

Prestack imaging refers to the process by which energy distributed over Cheop's pyramid is collapsed back to the scatterpoint location at the pyramid's apex. Full prestack Kirchhoff migration directly sums all energy on Cheop's pyramid to the apex. In contrast, dip moveout (DMO) processing using NMO, DMO, and inverse NMO or Gardner's DMO (Gardner et al. 1986) conceptually reshapes the data in Cheop's pyramid to a hyperboloid, which is NMO corrected, stacked, and imaged with poststack migration. Conventional processing based on CMP gathers is forced

to ignore the non-hyperbolic shape of Cheop's pyramid, which limits imaging in structured areas.

In addition to kinematic summation (using the DSR equation), Kirchhoff imaging requires the scaling, antialias filtering, and phase filtering of the input data for every input sample (Gazdag and Squazzero 1984, Silva 1992, Lumley and Claerbout 1993, Lumley et al. 1994). These intermediate operations account for a significant proportion of the computational expense of the migration process.

Prestack migration gathers

Due to practical and historical reasons, conventional processing has attempted to collapse the energy on Cheop's pyramid in two kinematic steps; NMO removal and poststack migration. These steps require two different velocities. In contrast, full prestack Kirchhoff time migration uses a single focusing operation with one velocity function that is defined at the apex of Cheop's pyramid. Finding this prestack migration velocity has been an elusive goal. Stolt and Benson (1986, page 36) expressed the desire for an operator "which migrates the unstacked data but leaves NMO and stack undone". In a subsequent figure (Stolt and Benson 1986, Figure 1.17) a prestack migration gather is illustrated in which the input traces are sorted by offset. Velocities defined from such a gather should yield the prestack migration velocities.

Forel and Gardner (1988) describe a Fourier method based on DMO before NMO to form prestack migration gathers. More recently Ferber (1994) described an alternate time domain method that is based on Gardner's DMO. These and other methods create prestack migration gathers with very high fold and with apparent offsets that can be much greater than the maximum source receiver offset. The very high fold is due to the binning of all input traces within the migration aperture into the prestack migration gather. Such gathers allow more accurate velocity analysis than is possible with conventional CMP gathers.

THE EQUIVALENT OFFSET AND COMMON SCATTERPOINT (CSP) GATHERS

The equivalent offset

The *equivalent offset* is defined by converting the DSR equation (3) into an equivalent single square root or hyperbolic form. This is accomplished by defining a new source and receiver *collocated* at the equivalent offset position E in Figure 3. The equivalent offset is chosen to maintain the same total traveltime $2T_e$ as the original path T , i.e.,

$$T = T_s + T_r = 2T_e . \quad (5)$$

Equating the traveltime for the equivalent offset raypath with the DSR equation we get

$$T = \left[\left(\frac{T_0}{2} \right)^2 + \frac{(x+h)^2}{V_{mig}^2} \right]^{1/2} + \left[\left(\frac{T_0}{2} \right)^2 + \frac{(x-h)^2}{V_{mig}^2} \right]^{1/2} = 2T_e = 2 \left[\left(\frac{T_0}{2} \right)^2 + \frac{h_e^2}{V_{mig}^2} \right]^{1/2}, \quad (6)$$

where we may solve for the equivalent offset h_e (Appendix 1) to get

$$h_e^2 = x^2 + h^2 - \left(\frac{2xh}{TV_{mig}} \right)^2. \quad (7)$$

This equation is roughly a quadratic sum of the distance between the CSP and the CMP x , and the half source-receiver offset h . The bracketed term in equation (7) contributes a small time and velocity dependence to the equivalent offset.

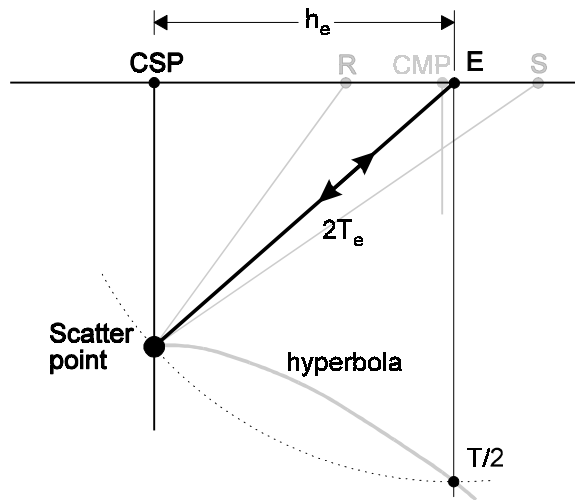


FIG. 3. Illustration of prestack migration showing the equivalent offset position E for a collocated source and receiver. Compare to Figure 1.

Common scatterpoint gathers

Equation (6) shows that scattered energy from a particular scatterpoint, when considered as a function of equivalent offset, will be distributed along a hyperbolic path. Thus a new type of prestack migration gather can be formed by ordering all traces according to their equivalent offset from a presumed scatterpoint location. We call such gathers *common scatterpoint (CSP) gathers*. Energy in each input trace is copied directly to all CSP gathers (within the migration aperture) *without* time shifting.

In practice the equivalent offset is quantized to discrete bins and all energy which falls into a bin is summed. A consequence of the time-varying equivalent offset (equation 7) is that an input trace may have its samples spread over a number of offset bins (Figure 4). The first useful energy in an input trace comes from a zero depth scatterpoint at the CSP location and has an equivalent offset $h_{e\alpha}$ defined by

$$h_{e\alpha} = x. \quad (8)$$

The starting time T_α of this useful energy is given by

$$T_\alpha = \frac{2h_{e\alpha}}{V_0}, \quad (9)$$

where the velocity at the surface ($T_0 = 0$) is given by V_0 . Energy at this point will migrate to the surface at the CSP location with a dip of 90 degrees.

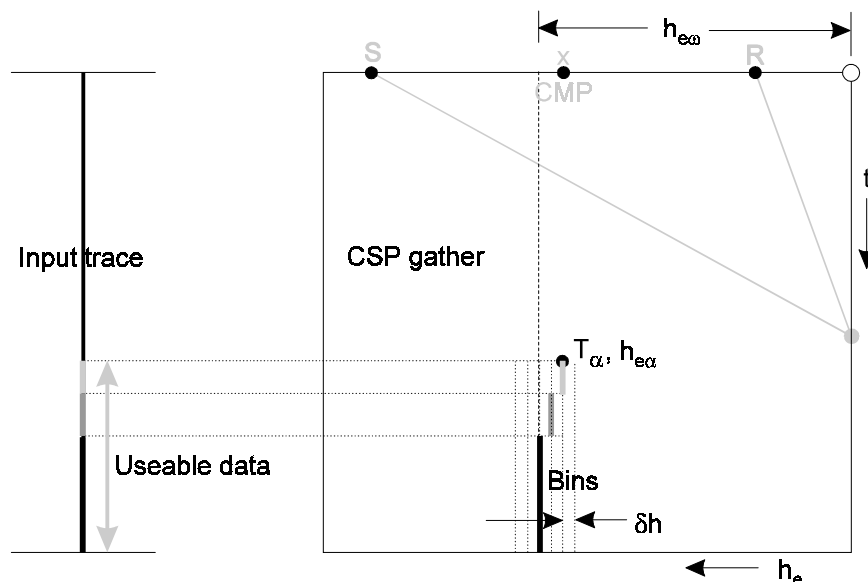


FIG. 4. Illustration of data mapping from an input trace to bins in a CSP gather. Only a portion of the input trace is useable for this CSP gather and is identified by the various levels of gray. The data mapping occurs at constant time.

When the input time tends to a large value, the equivalent offset tends to a vertical asymptote $h_{e\omega}$ given by

$$h_{e\omega}^2 = x^2 + h^2, \quad (10)$$

as illustrated in Figure 4. In some cases, the number of offset bins for a given input trace may be reduced to one bin at offset $h_{e\omega}$. This benefit also occurs when either x or h are small, or when the first useful scatterpoints are well below the surface as in marine data.

It may appear from equation (7) that the equivalent offset needs to be computed for each input sample. However, because the CSP gather is formed by compositing traces into equivalent offset bins, only times at which the input samples start in a new bin need to be computed. The initial equivalent offset $h_{e\alpha}$ may be computed using equation (8) and assigned to an appropriate bin. The following samples are added to this bin until the equivalent offset increases to the bin boundary at which point the input samples are added to the next bin. The time at which these transitions occur is T_n , where n is the bin index, and may be found from rearranging equation (7) to give

$$T_n = \frac{(2xh)}{V_{mig} [x^2 + h^2 - h_{en}^2]^{1/2}}, \quad (11)$$

where h_{en} is the equivalent offset of the n^{th} bin boundary. The transition times of each offset bin for a given input trace may be computed to allow efficient copying of the samples into the respective bins. In practice the time dependence of velocity at T_0 must be addressed in equations (7) and (11) as is the case with all NMO applications.

Extension to 3-D data

In a 3-D world where velocities vary only with z , the traveltimes for scattered energy depends only on the distances from the source and receiver to the scatterpoint and not on their relative azimuths. This symmetry can be exploited to extend equivalent offset concepts to 3-D in a way appropriate for time migration. A plan view of a source S , scatterpoint CSP , and receiver R is shown in Figure 5, with source to scatterpoint offset h_s , and the scatterpoint to receiver offset h_r . Converting this 3-D geometry to a 2-D geometry is accomplished by rotating the vertical planes containing these source and the receiver raypaths into a common vertical plane (with an arbitrary azimuth), also illustrated in Figure 5. Values of x and h are now computed from scalar values of h_s and h_r , i.e.,

$$x = \frac{h_s + h_r}{2}, \quad (12)$$

and

$$h = \frac{|h_s - h_r|}{2}. \quad (13)$$

When inserted into equation (7), these equations allow the computation of a 3-D equivalent offset. The geometry in the common plane is *not* directly related to the original source receiver offset or the CMP location of the 3-D geometry. Azimuthal information of the original source and receiver raypaths will be lost, but could be preserved if required.

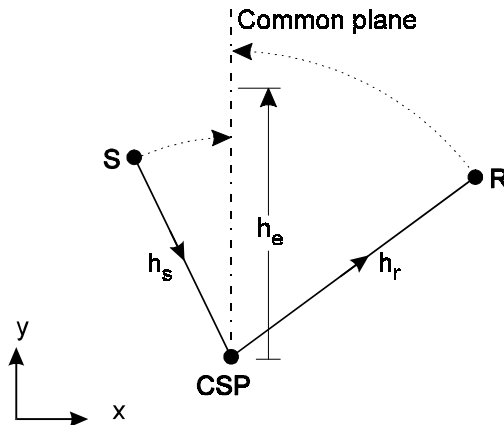


FIG. 5. Plan view of a 3-D showing a source S receiver R and a CSP location. To compute the equivalent offset h_e , the vertical planes containing the source and receiver raypaths are rotated to a common plane

of the travelttime differential is used in CSP velocity analysis. An alternate view is that CSP velocity analysis is based on the distances from the source and receivers to the CSP location, and not on the source/receiver offset, thus leading to a more natural method of processing.

The equivalent offset is time and velocity dependent (equation (7)); however, many samples are summed into a CSP gather using only the asymptotic equivalent offset $h_{e\omega}$ (which is independent of both time and velocity), providing stability to the CSP gathering process when the velocities are unknown. The CSP gathers may be formed at a few locations with an estimated velocity, and the gather used to define more accurate velocities. The iterations of this process converge very rapidly (Bancroft and Geiger 1996), and usually only one is required. Velocities derived from the CSP gather are imaging velocities which approximate RMS velocities, and therefore tie reasonably with sonic logs.

The increased offset range and high fold of the CSP gather improves the resolution of velocity semblance plots compared to those obtained from a conventional super CMP gather (formed by stacking adjacent CMP gathers). The improved focusing of CSP energy illustrates the increased resolving power of prestack migration, and the requirement that velocities must be quite accurate (less than a few percent error) to maximize the migrated energy. In addition, the CSP gather is formed at one location and preserves the velocity information of dipping events, which is in contrast to the super CMP gather which mixes the dipping information across the midpoint range of the contributing CMPs.

The resolution of long path multiples is also improved in the CSP gather, which suggests that full prestack migration will produce better multiple attenuation than conventional processing. The fold of the gathers and the differential moveout between multiples and primaries are the key determinants of multiple attenuation. Both of these factors are generally greater for CSP gathers than CMP gathers.

The CSP gathers should not be confused with CMP gathers formed after migration of constant offset sections or shot records. The latter techniques sort the migrated traces into CMP gathers where inverse NMO is applied as in Yilmaz (1987 section 4.4.1). Theoretically the migrated traces are at zero offset; therefore the offset used in the inverse NMO is somewhat arbitrary. The resolution of the resultant velocity scans will be limited by the source-receiver offset as with unmigrated CMP gathers. In addition, errors in the initial guess velocities result in unresolved spatial positioning errors. We believe that this method of velocity analysis is less robust and converges more slowly than the equivalent offset method.

Processing and imaging CSP gathers

After the formation of CSP gathers, the remaining processing steps to complete the prestack migration are scaling, filtering, NMO removal, and stacking. Taken together, these steps form the imaging process which is equivalent to a Kirchhoff migration of the CSP gathers to an output zero offset trace. Regular processing

software may be used, along with conventional velocity analysis techniques. The only new algorithms required are those which form the CSP gather.

The efficiency of Kirchhoff migrations is increased by postponing as much scaling and filtering as possible until after the summation process (Silva 1992). In our companion paper (Margrave et al. 1996) theoretical scaling factors are shown to be a function of (x, h, h_e) , suggesting that some scaling may be required prior to equivalent offset binning. However in practice, it appears sufficient to postpone all scaling and filtering until after the formation of the binned traces in the CSP gathers. Thus it becomes economical to apply accurate antialiasing and phase shifting filters before NMO, and to apply scaling prior to final imaging. Once the CSP gathers have been formed, migration parameters (such as dip range, scaling, and filtering) may be evaluated by forming fully migrated images. In addition, any signal enhancement process may be applied to the CSP gathers prior to imaging. The high fold and full range of offsets in the CSP gathers enable these algorithms to perform more effectively than on CMP gathers.

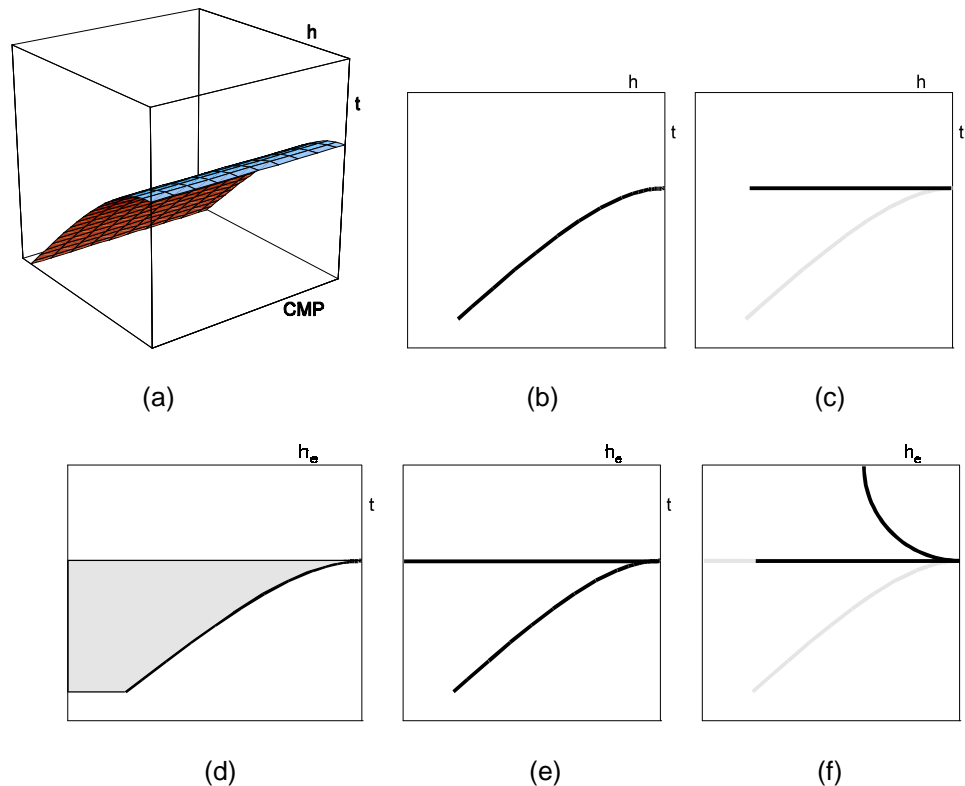


FIG. 7. Prestack migration volume for a 2-D horizontal reflector is shown in (a). Figures (b) through (f) show various kinematic views of CMP and CSP gathers, with (b) a CMP gather before NMO, (c) the application of NMO to the CMP gather, (d) a CSP gather with the gray area showing distribution of energy which cancels to give results in (e) showing the hyperbolic and horizontal energy and (f) the application of NMO to the CSP gather. The above discussion is purely kinematic. Energy from a horizontal reflector is concentrated around the apex of the hyperbola in Figure 7e. For a dipping reflector, the energy is concentrated down the limb of the hyperbola at an equivalent offset defined by the normal incidence ray.

Example of planar reflections

A CSP gather combines a great deal more data than a CMP gather and is considerably different. As previously discussed, the CSP gather for an isolated scatterpoint at $x = 0$ maps the entire 3-D (x, h, t) Cheep's pyramid into a hyperbola in (h_e, t) at $x = 0$. Figure 7 illustrates the mapping for the case of an ideal horizontal reflector. The input traveltime surface is the hyperbolic sheet shown in Figure 7a. A CMP gather is a vertical slice at constant x_{cmp} through the sheet as shown in 7b. NMO applied to 7b results in 7c. The CSP mapping can be visualized (approximately) by rotating each point on the sheet at constant time (as illustrated in Figure 6) to its asymptotic equivalent offset (equation 10). The resulting CSP gather is shown in 7d. Energy in 7d is spread through the gray region, where band limited constructive and destructive interference restricts most energy to the boundaries as shown in 7e. NMO applied to 7e results in 7f. Stacking 7f will produce a strong event at the horizontal reflector, but complete imaging requires the wavelet phase shaping of Kirchhoff migration to account for NMO stretch and circular moveout of the horizontal event.

Natural anti-aliasing filters

Energy from a scatterpoint will map to a hyperbola on a CSP gather as illustrated in Figure 8. When binned, the data becomes smeared across a bin width δh which is equivalent to convolving the input data at constant time with a spatial boxcar filter of width δh . This is the well known array effect which attenuates higher frequencies at steeper dips (Sheriff and Geldart 1995 section 8.3.5). This filter may appear to be a detriment to the process, but is actually a benefit. It has similar properties to a temporal filter which attenuates spatially aliased frequencies as required for Kirchhoff migration. In effect, it provides a natural antialiasing filter for the data in a CSP gather.

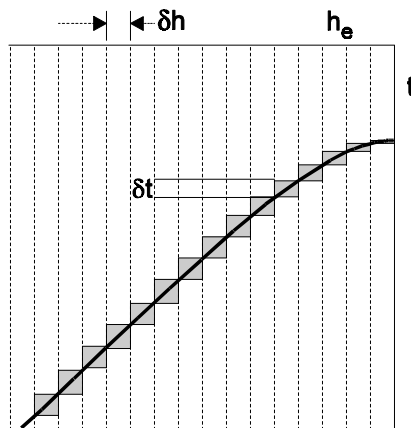


FIG. 8. A hyperbolic event in a CSP gather with bins of width δh . The CSP binning process gathers data to the center of each bin resulting in a spatial and temporal smear over δh and δt .

EXAMPLES OF PROCESSING

A number of examples have been included to compare CSP gathers with CMP gathers, and to illustrate the results that are obtained. The first example is a comparison of CSP and CMP gathers taken from a marine line, the second set of examples come from a 2-D land line featuring a erosional channel, and the third set uses a land 3-D dataset featuring a pinnacle reef. Prior to EOM, the datasets have been corrected to a flat datum using statics estimated by conventional processing. Trace amplitudes in the CSP gathers have been adjusted to aid in visualization.

Marine example

The data featured in Figure 9 is extracted from a marine line and shows in (a) an super CMP gather, and (b) a two sided CSP gather. Half offsets for the super CMP gather range from 200 to 1330 m. while the equivalent offsets for the CSP gather range from -5000 m to 5000 m. The fold in each offset bin of the super CMP gather is one, achieved by summing eight adjacent CMP locations, while the average fold across the CSP gather is approximately 15.

Since the water bottom is close to 3 seconds, the CSP gather was formed using only the asymptotic equivalent offset $h_{e\omega}$ enabling each input trace to be summed into one offset bin. Hyperbolic information is visible to larger offsets. Dipping energy may be observed at offsets beyond the range of the CMP gather, as identified by the arrow in Figure 9b.

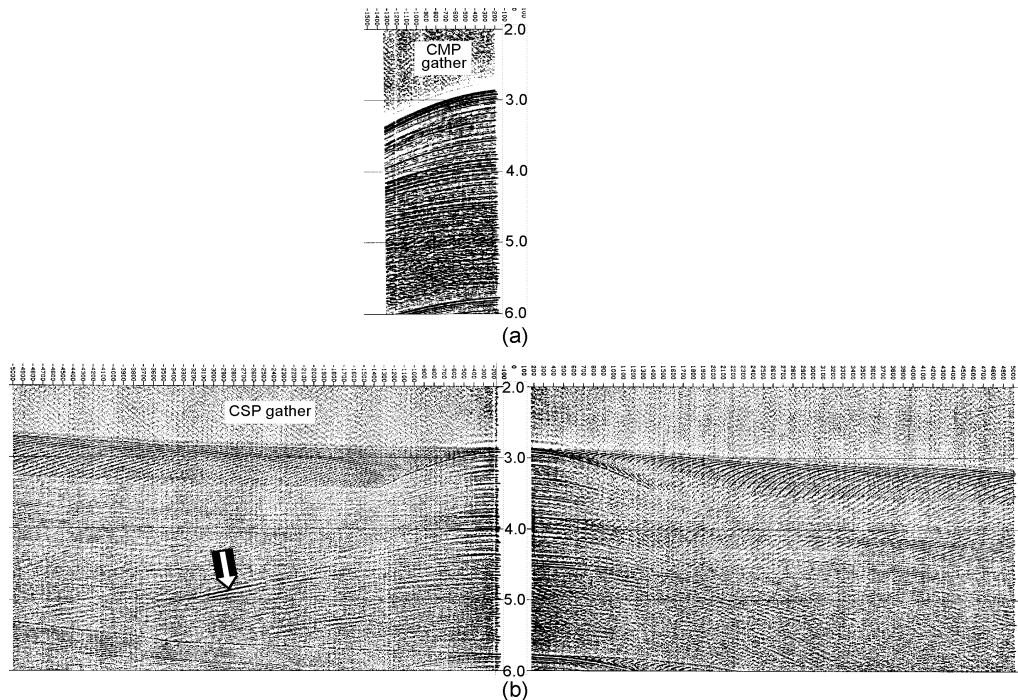


FIG. 9. A marine 2-D example with (a) showing a CMP gather and (b) a CSP gather. The arrow identifies energy from a dipping reflector at the CSP location that is not imaged in the CMP gather.

The CSP gather also contains structural information as evident by the sloping water bottom. Much of the structural energy in this CSP gather is above the first useful time T_{α} and would be removed by the NMO process. Energy above T_{α} is aliased contributing to the noise patterns that are visible.

2-D land line featuring an erosional channel

Figure 10 contains three panels: a conventional CMP gather of traces sorted by offset, a CMP gather with traces positioned at the actual source-receiver offset (labeled CMPX), and a CSP gather. The gathers are all located over the flank of a sand filled erosional channel at $T_0 = 1.2$ s. Note the increased coverage and data at larger offsets in the CSP gather. Dipping energy of the channel may be observed on the CSP gather at $T = 1.3$ s (see arrow), but is not evident on the CMP gather.

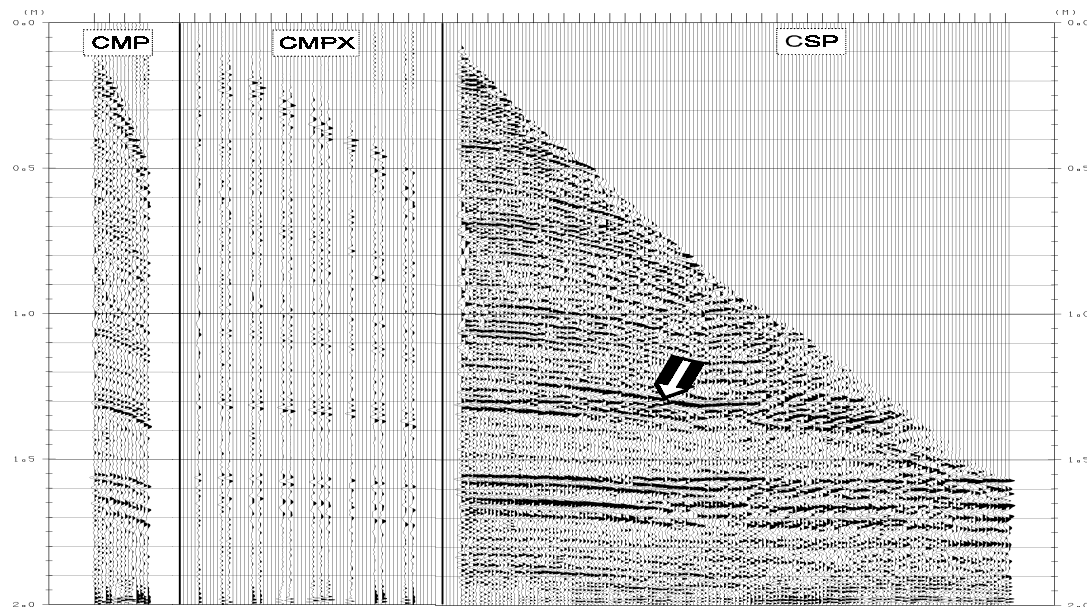


FIG. 10. A channel sand example showing a CMP gather, a CMP gather with traces located at the actual source-receiver offsets (CMPX), and a CSP gather. Note the lack of coverage in the CMPX gather, and the full coverage with increased offsets in the CSP gather. The arrow identifies the reflection from the dipping flank of the sand channel.

Velocity analysis semblance plots are shown in Figure 11 at the location of Figure 10 for (a) a super CMP gather and (b) a CSP gather. The super CMP gather (not shown) was formed from six CMP gathers to fill the missing offsets. Note the improved velocity resolution of the CSP gather for primaries and multiples.

Figure 12 compares (a) the stacked section of the channel with (b) a conventional poststack migration and (c) an EOM image. Figure 12c shows improved signal coherence and we believe it is more interpretable than Figure 12b.

Figure 13 shows a 2-D line extracted from a 3-D dataset that contains a pinnacle reef, with (a) the stacked section (b) a conventional prestack 3-D migration using stacking velocities, and (c) the 3-D EOM image using velocities determined from the

CSP gathers. The EOM image shows improvements in coherence, detail, and spatial resolution.

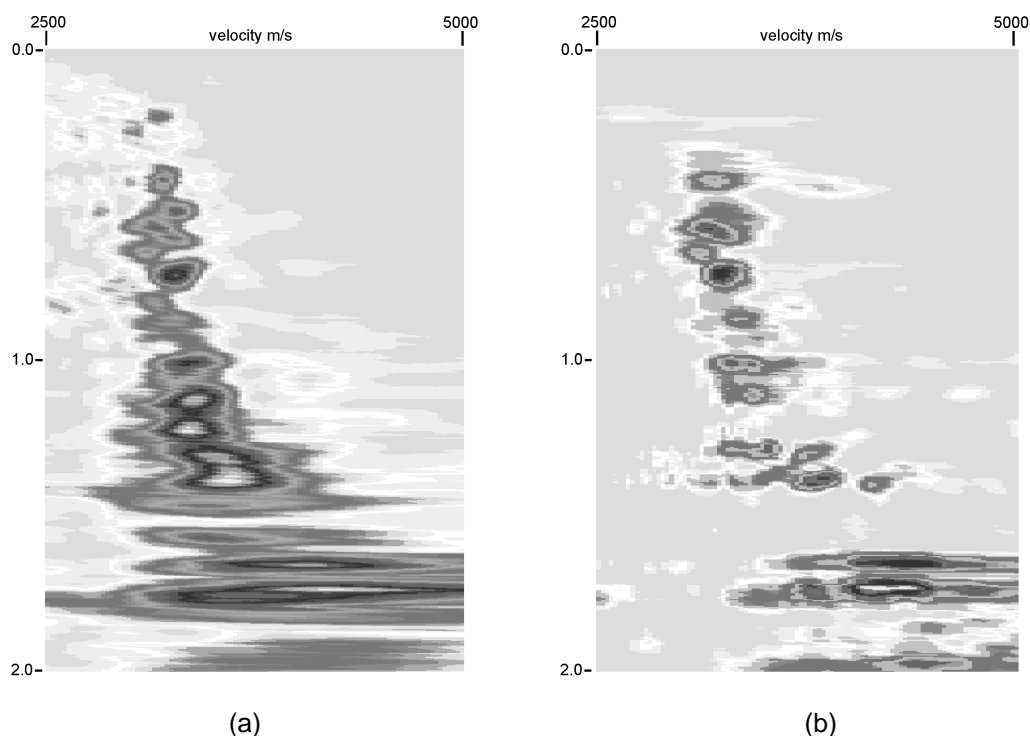


FIG. 11. Semblance plots for (a) a super CMP gather and (b) the CSP gather in Figure 10. The super CMP gather was formed by compositing six CMP gathers around the CMP gather in Figure 10. Note the improved focusing on the CSP gather.

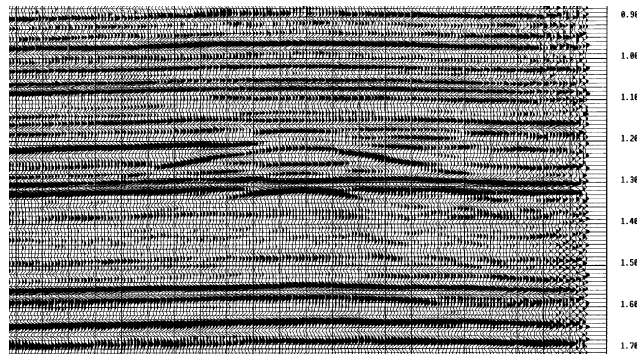
ADDITIONAL BENEFITS OF EQUIVALENT OFFSET MIGRATION

The equivalent offset method of prestack migration has a number of benefits that have been demonstrated but not included in this paper. The first of these benefits is its ability to migrate data from an irregular surface (Geiger and Bancroft 1996). Any Kirchhoff migration may be modified to enable migration from topography by including the velocity changes with elevation. Migration from topography enables a more accurate imaging and reduces static errors due to elevation corrections.

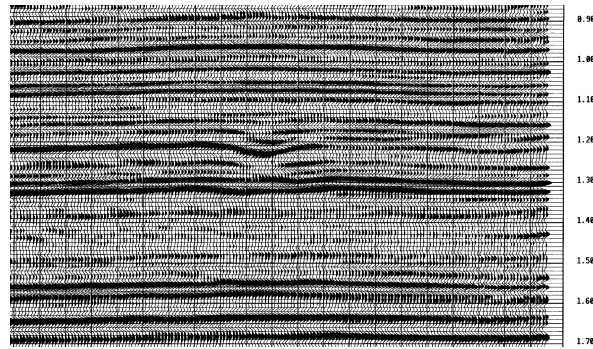
The ability of full prestack migration to focus and collect all the migratable energy, increases the signal to noise ratio (SNR), especially at the higher frequencies. This allows additional spectral whitening after migration for improved bandwidth and wavelet resolution.

The process of EOM may be applied to converted wave data. Converted waves have a P wave velocity from the source to the scatter point (or conversion point), and an S wave velocity from the scatter point to the surface. Conventional processing of this P-SV data has been quite difficult, but Bancroft and Wang (1994) and Wang et al. (1995) extended the concept of equivalent offset to include the appropriate P and S

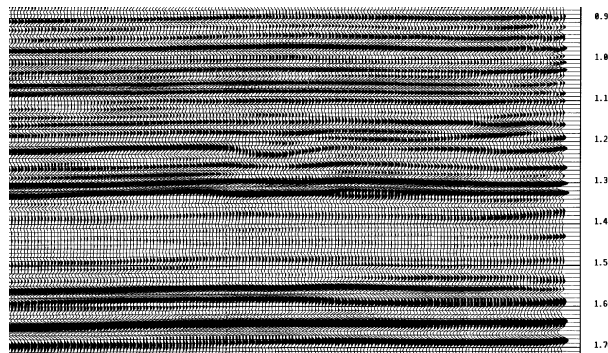
wave velocities. The converted wave CSP gathers show hyperbolic moveout and are imaged by an EOM process.



(a)



(b)



(c)

FIG. 12. Comparison of (a) a stacked section, (b) poststack migration, and (c) an EOM for the channel sand located at 1.2 s.

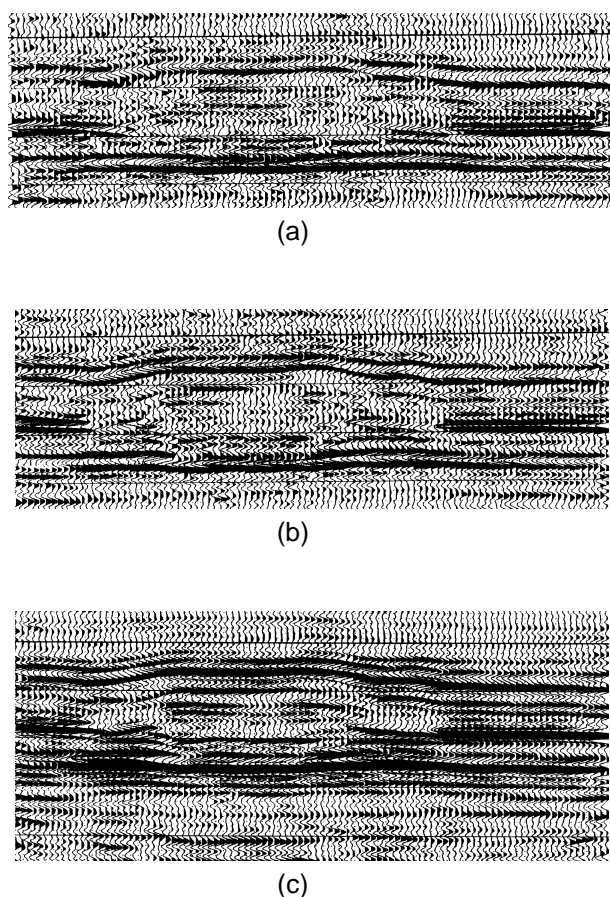


FIG. 13. A 2-D line extracted from a 3-D dataset showing a pinnacle reef with (a) the stacked section, (b) a conventional prestack migration using stacking velocities and (c) the EOM using velocities determined from the CSP gathers.

CONCLUSIONS

A robust method of prestack migration has been developed that is simpler and much faster than conventional methods. This is accomplished by using the *equivalent offset* which converts the prestack double square root equation into a single square root equation. Energy from all input traces within the prestack migration aperture are summed into the common scatter point (CSP) gather with offsets defined by the equivalent offset. No time shifting of the input data is required. Antialias filtering, scaling, and the phase-shifting filter are postponed until after the gather has been formed for a significant savings in computation time. Scattered energy in the CSP gathers lies on hyperbolic paths, suitable for conventional velocity analysis, after which the Kirchhoff migration steps of scaling, filtering, NMO, and stacking, complete the prestack migration. The formation of the CSP gathers provides additional benefits by allowing additional scaling and or 2-D filtering before the final migration step.

Advantages of the method include extremely fast processing times, accurate velocity analysis, and simplified processing. The process may be adapted for rugged topography, or applied to converted wave processing.

Inserting the method into a processing system is straight forward as only the CSP gather algorithm needs to be developed. Conventional processing tools provide the remaining steps, similar to processing CMP gathers to a stacked section.

ACKNOWLEDGMENTS

We wish to thank the sponsors of the CREWES Project for their support and are grateful for additional assistance from Lithoprobe. The technical support from Henry Bland was greatly appreciated. We also express our gratitude to Husky Oil, Mobil Oil, Ulterra, and C and C Systems, all of Calgary, for the use of the examples included in this paper.

REFERENCES

- Bancroft, J. C., and Geiger, H. D., 1994, Equivalent offsets and CRP gathers for prestack migration: 64th Ann. Internat. Mtg. Soc. Expl. Geophys., Expanded Abstracts, 672-675.
- Bancroft, J. C., Geiger, H. D., Foltinek, D. S., and Wang, S., 1994 Prestack migration by equivalent offsets and CSP gathers, CREWES 1994 Research Report.
- Bancroft, J. C., and Wang, S., 1994, Converted-wave prestack migration and velocity analysis by equivalent offsets and CSP gathers, CREWES 1994 Research Report.
- Bancroft, J. C., Wang, S., Foltinek, D. S., and Geiger, H. D., 1995, Common scatterpoint (CSP) prestack migration: CSEG National Convention, Expanded Abstracts, 47-48.
- Bancroft, J. C., and Geiger, H. D., 1996, Velocity sensitivity for equivalent offset prestack migration: a contrast in robustness and fragility: CSEG National Convention, Expanded Abstracts, 149-150.
- Black, J. L., and Brzostowski, M. A., 1991, Steep-dip time migration and residual depth migration: 61st Ann. Internat. Mtg. Soc. Expl. Geophys., Expanded Abstracts, 1140-1143.
- Claerbout, J. F., 1984, Imaging the Earth's Interior: Blackwell Scientific
- Deregowski, S., 1986, What is DMO?: First Break, **4**, 7-24
- Deregowski, S. M., 1990, Common-offset migrations and velocity analysis: First Break, **8**, 225-234
- Denelle, E., Dezard, Y., and Raoult, J. J., 1986, 2-D prestack depth migration in the (S-G-W) domain: 56th Ann. Internat. Mtg. Soc. Expl. Geophys., Expanded Abstracts, 327-330
- Diet, J. P., Audebert, F., Huard, I., Lanfranchi, P., and Zhang, X., 1993, Velocity analysis with prestack time migration using the S-G method: A unified approach: 65th Ann. Internat. Mtg. Soc. Expl. Geophys., Expanded Abstracts, 957
- Dix, C. H., 1955, Seismic velocities from surface: Geophysics, **20**, 86-86
- Ferber, R. G., 1994, Migration to multiple offset and velocity analysis: Geophy. Prosp., **42**, 99-112
- Forel D. and Gardner, G., 1988, A Three-Dimensional Perspective on Two-Dimensional Dip Moveout: Geophysics, **53**, 604-610
- Gardner, L. W., 1947, Vertical velocities from reflection shooting: Geophysics, **12**, 221-228
- Gardner, G. H. F., Wang, S. Y., Pan, N. D., and Zhang, Z., 1986, Dip moveout and prestack imaging:, Offshore Technology Conference.
- Gazdag, J., and Squazzero, P., 1984, Migration of Seismic Data: Proceedings of IEEE.
- Geiger, H., Bancroft, J. C. and Foltinek, D., 1995, Prestack migration of crustal data using common scatterpoint (CSP) migration technique: Expanded Abstracts CSEG 1995 National Convention

- Geiger, H., Bancroft, J. C., 1996, Equivalent offset prestack migration - application to rugged topography and formation of unmigrated zero offset section: EAGE 58th Conference Extended Abstracts, P098.
- Hale, D., 1984, Dip Move-out by Fourier transform: *Geophysics*, **49**, 741-757.
- Hubral, P., and Krey, T., 1980, Interval Velocities from Seismic Reflection Time Measurements: Society of Exploration Geophysicists.
- Lee, W. B. and Zhang, L., 1992, Residual shot profile migration: *Geophysics*, **57**, 815-822
- Lindsey, J. P., and Herman, A., 1970, Digital migration, *Oil and Gas Journal*, **38**, 112-115
- Lumley, D. E., 1989, A generalized Kirchhoff-WKB depth migration theory for multi-offset seismic reflection data: reflectivity model construction by wavefield imaging and amplitude estimation: M.Sc. thesis, Univ. of British Columbia
- Lumley, D. E., and Claerbout, J. F. 1993, Anti-aliased Kirchhoff 3-D migration: a salt intrusion example: SEG 3-D Seismic Workshop, 115-123
- Lumley, D. E., Claerbout, J. F., and Bevc, D., 1994, Anti-aliased Kirchhoff 3-D migration: , 1282-1285
- Margrave, G. F., Bancroft, J. C., and Geiger, H., 1996; The theoretical basis for prestack migration by equivalent offset: *Geophysics*, (submitted)
- Mayne, W. H., 1962, Common-reflection-point horizontal data stacking techniques: *Geophysics*, **27**, 927-938
- Ng, M., 1994, Prestack migration of shot records using phase shift plus interpolation: *Canadian Journal of Exploration Geophysics*, **30**, 11-27
- Reshef, M., and Kosloff, D., 1986, Migration of Common-Shot Gathers: *Geophysics*, **51**, 324-331.
- Rockwell, D. W., 1971, Migration stack aids interpretation: *Oil and Gas Journal*, **69**, 202-218
- Sattlegger, J. W., Stiller, P. K., Echterhoff, J. A. and Hentschke, M. K., 1980, Common offset plane migration (COPMIG): *Geophys. Prosp.*, **28**, 859-871
- Schultz, P. and Sherwood, 1980, Depth migration before stack: *Geophysics*, **45**, 376-393
- Sheriff, R. E., and Geldart, L. P., 1995, *Exploration Seismology*: Cambridge University Press
- Silva, R., 1992, Antialiasing and application of weighting factors in Kirchhoff migration: Technical Program, 62nd Ann. Internat. Mtg. Soc. Expl. Geophys., 995-998
- Stolt, R., 1978, Migration by Fourier transform: *Geophysics*, **43**, 23-48.
- Stolt, R. H., and Benson, A. K., 1986, *Seismic migration, theory and practice*: Geophysical Press
- Taner, M. and Koehler, F., 1969, Velocity spectra-digital computer derivation and applications of velocity functions: *Geophysics*, **34**, 859-881.
- van der Schoot, A., Romijn, R., Larson, D. E., and Berkhout, A. J., 1989, Prestack migration by shot record inversion and common depth point stacking: a case study: *First Break*, **7**, 293-304
- Wang, S., Bancroft, J. C., Foltinek, D., and Lawton, D., 1995, Converted -wave (P-SV) prestack migration and velocity analysis: Expanded Abstracts CSEG 1995 National Convention
- Yilmaz, O., 1987, *Seismic Data Processing*: SEG.

APPENDIX 1. DERIVATION OF THE EQUIVALENT OFFSET EQUATION (7)

Starting with equation (6), and using V as the migration velocity at T_o , we get

$$\left[\left(\frac{T_0 V}{2} \right)^2 + (x+h)^2 \right]^{\frac{1}{2}} = 2 \left[\left(\frac{T_0 V}{2} \right)^2 + h_e^2 \right]^{\frac{1}{2}} - \left[\left(\frac{T_0 V}{2} \right)^2 + (x-h)^2 \right]^{\frac{1}{2}} \quad (\text{A1})$$

then by squaring both sides of the equation,

$$\begin{aligned} \left(\frac{T_0 V}{2} \right)^2 + (x+h)^2 &= 4 \left[\left(\frac{T_0 V}{2} \right)^2 + h_e^2 \right] + \left[\left(\frac{T_0 V}{2} \right)^2 + (x-h)^2 \right] - \\ &4 \left\{ \left[\left(\frac{T_0 V}{2} \right)^2 + h_e^2 \right] \left[\left(\frac{T_0 V}{2} \right)^2 + (x-h)^2 \right] \right\}^{\frac{1}{2}} \end{aligned} \quad (\text{A2})$$

expanding terms

$$\begin{aligned} \left(\frac{T_0 V}{2} \right)^2 + x^2 + h^2 + 2xh &= 4 \left[\left(\frac{T_0 V}{2} \right)^2 + h_e^2 \right] + \left(\frac{T_0 V}{2} \right)^2 + x^2 + h^2 - 2xh - \\ &4 \left\{ \left[\left(\frac{T_0 V}{2} \right)^2 + h_e^2 \right] \left[\left(\frac{T_0 V}{2} \right)^2 + (x-h)^2 \right] \right\}^{\frac{1}{2}} \end{aligned} \quad (\text{A3})$$

to get

$$\begin{aligned} 4xh &= 4 \left[\left(\frac{T_0 V}{2} \right)^2 + h_e^2 \right] - \\ &4 \left\{ \left[\left(\frac{T_0 V}{2} \right)^2 + h_e^2 \right] \left[\left(\frac{T_0 V}{2} \right)^2 + (x-h)^2 \right] \right\}^{\frac{1}{2}} \end{aligned} \quad (\text{A4})$$

resorting,

$$\left[\left(\frac{T_0 V}{2} \right)^2 + (x-h)^2 \right]^{\frac{1}{2}} = \frac{4 \left[\left(\frac{T_0 V}{2} \right)^2 + h_e^2 \right] - 4xh}{4 \left[\left(\frac{T_0 V}{2} \right)^2 + h_e^2 \right]^{\frac{1}{2}}} \quad (\text{A5})$$

simplifying

$$\left[\left(\frac{T_0 V}{2} \right)^2 + (x-h)^2 \right]^{\frac{1}{2}} = \left[\left(\frac{T_0 V}{2} \right)^2 + h_e^2 \right]^{\frac{1}{2}} - \frac{xh}{\left[\left(\frac{T_0 V}{2} \right)^2 + h_e^2 \right]^{\frac{1}{2}}} \quad (\text{A6})$$

squaring

$$\left(\frac{T_0V}{2}\right)^2 + x^2 + h^2 - 2xh = \left(\frac{T_0V}{2}\right)^2 + h_e^2 + \frac{(xh)^2}{\left[\left(\frac{T_0V}{2}\right)^2 + h_e^2\right]} - 2xh \quad (\text{A7})$$

eliminating terms, and resorting

$$h_e^2 = x^2 + h^2 - \frac{(xh)^2}{\left[\left(\frac{T_0V}{2}\right)^2 + h_e^2\right]} \quad (\text{A8})$$

and finally, the denominator term is simplified with the total two way time T to get the desired result.

$$h_e^2 = x^2 + h^2 - \left(\frac{2xh}{TV}\right)^2 \quad (\text{A9})$$